One-Step Synthesis of SnO 2 and TiO 2 Hollow Nanostructures with Various Shapes and Their Enhanced Lithium Storage Properties

ARTICLE *in* CHEMISTRY - A EUROPEAN JOURNAL · JUNE 2012

Impact Factor: 5.73 · DOI: 10.1002/chem.201103842 · Source: PubMed

4 AUTHORS, INCLUDING:

Zhiyu Wang
Dalian University of Technology
53 PUBLICATIONS **3,242** CITATIONS

SEE PROFILE

CHEMISTRY
A EUROPEAN JOURNAL

FULL PAPER

DOI: 10.1002/chem.201103842

One-Step Synthesis of SnO_2 and TiO_2 Hollow Nanostructures with Various Shapes and Their Enhanced Lithium Storage Properties

Zhiyu Wang,[a, b] Zi Chen Wang,[a] Srinivasan Madhavi,*[b] and Xiong Wen (David) Lou*[a]

Abstract: A versatile one-step method for the general synthesis of metal oxide hollow nanostructures is demonstrated. This method involves the controlled deposition of metal oxides on shaped α-Fe_2O_3 crystals which are simultaneously dissolved. A variety of uniform SnO_2 hollow nanostructures, such as nanococoons, nanoboxes, hollow nanorings, and nanospheres, can be readily generated. The method is also applicable to the synthesis of shaped TiO_2 hollow nanostructures. As a demonstration of the potential applications of these hollow nanostructures, the lithium storage capability of SnO_2 hollow structures is investigated. The results show that such derived SnO_2 hollow structures exhibit stable capacity retention of 600–700 $mAh\,g^{-1}$ for 50 cycles at a 0.2 C rate and good rate capability at 0.5–1 C, perhaps benefiting from the unique structural characteristics.

Keywords: electrochemistry · lithium-ion batteries · nanostructures · template synthesis · tin dioxide

Introduction

Hollow nanomaterials have attracted considerable attention from both fundamental research and technological aspects due to their large surface area, usable nanoscale interiors, low density, and in some cases good surface permeability compared with solid materials.[1] Prompted by the great promise in myriad applications, such as photonic devices, energy storage, drug carriers, and nanoscale reactors, tremendous efforts have been invested in the synthesis of hollow nanostructures with desirable composition and structural complexity.[2–23] The most common routes towards hollow structures involve the growth of a shell of designed materials onto various removable templates by controlled surface precipitation and subsequent selective removal of the template.[9–23] In principle, the utilization of pregrown templates allows one to discretionarily manipulate the morphology and interior structure of the resultant hollow structures for better control of the properties. However, the geometry of hollow products obtained in practice is mostly spherical and the synthesis of nonspherical hollow particles still suffers from many difficulties, ranging from the paucity of nonspherical templates available to less controllable coating around their high-curvature surfaces. Tedious procedures for template removal also bring additional problems to the product quality and process cost.

Recently, novel approaches based on sacrificial templates have been developed for the preparation of hollow structures of various materials, such as noble metals, transition-metal oxides, and sulfides, based on different principles, such as the Kirkendall effect, electroless galvanic replacement, and chemical etching.[16,20,24–29] Different from conventional strategies, the templates in these methods not only serve as the structure-directing scaffold, but also involve themselves as the consumable reactant for shell construction. In this regard, synthesis based on sacrificial templates is inherently advantageous because it generally requires no additional surface functionalization and shell formation is guaranteed by spontaneous chemical reaction. Therefore, this kind of technique is typically more efficient and economical, especially if the sacrificial template can be completely consumed during the simultaneous hollowing process.

As an important semiconducting metal oxide, SnO_2 has shown great potential in numerous applications, such as gas sensing and energy storage.[19,20,30–34] In view of their technological importance, various SnO_2 nanomaterials with structures ranging from zero-dimension nanoparticles to multidimensional assemblies have been synthesized by different methods.[9,17–20,23,30–57] For example, Zeng and co-workers have reported the self-construction of SnO_2 hollow octahedra through two-dimensional aggregation of nanocrystallites under hydrothermal conditions.[43] We have previously reported the synthesis of double-walled hollow nanostructures of SnO_2 by repeated shell-by-shell deposition of SnO_2 on silica templates and template-free fabrication of SnO_2

[a] Dr. Z. Wang, Z. C. Wang, Prof. X. W. Lou
School of Chemical and Biomedical Engineering
Nanyang Technological University
70 Nanyang Drive, 637457 Singapore (Singapore)
E-mail: xwlou@ntu.edu.sg

[b] Dr. Z. Wang, Prof. S. Madhavi
School of Materials Science and Engineering
Nanyang Technological University
50 Nanyang Avenue, 639798 Singapore (Singapore)
E-mail: madhavi@ntu.edu.sg

hollow spheres through hydrothermal routes.[19,23] By coordinating etching of cubic Cu_2O crystals, we recently demonstrated the fast production of high-quality SnO_2 nanoboxes at a low temperature.[20] An interesting strategy for the construction of SnO_2 hollow spheres was also developed in terms of molten-salt-mediated filling of mesoporous silica spheres and thermally induced restructuring.[17] Notwithstanding these advances, a general and facile route towards SnO_2 hollow nanostructures, in particular those with nonspherical shapes, is still highly desirable.

Herein, we present a general approach for one-pot synthesis of SnO_2 hollow nanostructures with different shapes by combining controlled deposition of SnO_2 from hydrolysis of $SnCl_2$ and simultaneous acidic etching of the sacrificial template. α-Fe_2O_3 crystals are selected as the templates because of their good material compatibility with SnO_2. Also, α-Fe_2O_3 is one of a very small number of inorganic materials that can be readily mass-produced in diverse sizes and shapes. Note that α-Fe_2O_3 is slowly dissoluble in an acidic solution at a relatively high temperature, hollow structures can in principle be generated as a result of simultaneous etching of α-Fe_2O_3 templates, and the deposition of shell materials is relatively fast. Encouragingly, a variety of nonspherical SnO_2 hollow nanostructures, including nanococoons, nanoboxes, and hollow nanorings, have been successfully generated by templating against shape-controlled α-Fe_2O_3 crystals under hydrothermal conditions. Remarkably, this approach can be easily extended to synthesize hollow structures of other metal oxides, such as TiO_2. Furthermore, the application of these SnO_2 hollow structures in lithium-ion batteries (LIBs) is also investigated. The results show that these SnO_2 hollow structures exhibit stable capacity retention of 600–700 mAh g^{-1} over 50 cycles at a current rate of 0.2 C.

Experimental Section

Synthesis of α-Fe_2O_3 nanotemplates: The α-Fe_2O_3 nanospindles were prepared by aging an aqueous solution of 20 mM $FeCl_3$ and 0.1 mM NaH_2PO_4 at 105 °C for 48 h.[58] The α-Fe_2O_3 nanocubes were obtained by storing an aqueous solution of 50 mM $FeCl_3$ at 160 °C for 12 h.[59] The α-Fe_2O_3 nanoparticles were synthesized by aging an aqueous solution of 23.7 mM $FeCl_3$ at 105 °C for 24 h.[59] The α-Fe_2O_3 nanorings were produced by treating a reaction solution of 20 mM $FeCl_3$, 0.18 mM NaH_2PO_4, and 0.55 mM Na_2SO_4 at 220 °C for 48 h.[60]

Synthesis of SnO_2 hollow nanostructures: For the synthesis of SnO_2 hollow nanostructures with various shapes, an appropriate amount of α-Fe_2O_3 crystals (e.g., 0.03 g of the nanospindles, or 0.02 g of the nanocubes, nanorings, or nanoparticles) was dispersed in deionized (DI) water (30 mL) by ultrasonication, followed by successively adding dilute hydrochloric acid (4 M, 3–4 mL) and $SnCl_2{\cdot}2H_2O$ powder (0.05 g) under constant magnetic stirring. After thorough mixing, the suspension was transferred into a 50 mL Teflon-lined stainless steel autoclave. The synthesis of SnO_2 nanococoons, nanoboxes, and hollow nanospheres was conducted at 180 °C for 20 h and the reaction for making SnO_2 hollow nanorings was carried out at 150 °C for 10 h. After reaction, the products were harvested by several rinse–centrifugation cycles with water and ethanol before being fully dried at 60 °C.

Synthesis of TiO_2 hollow nanostructures: The TiO_2 hollow nanostructures were synthesized by a similar procedure to that for making SnO_2 hollow structures except that $SnCl_2$ was replaced with TiF_4. Typically, α-Fe_2O_3 nanospindles or nanocubes (0.02 g) were dispersed in DI water (30 mL) by ultrasonication, followed by addition of dilute hydrochloric acid (4 M, 5 mL) and an aqueous solution of TiF_4 (0.02 M, 10 mL) under stirring. The reaction was carried out at 180 °C for 5 h in a 50 mL Teflon-lined stainless steel autoclave. After reaction, the products were collected by several rinse–centrifugation cycles with water and ethanol, and dried at 60 °C.

Material characterization: All the samples were characterized by field-emission scanning electron microscopy (FESEM, JEOL, JSM-7600F), transmission electron microscopy (TEM, JEOL, JEM-2010 and JEM-2100F), powder X-ray diffraction (XRD, Bruker, D8-Advance X-ray diffractometer, $Cu_{K\alpha}$), and nitrogen adsorption/desorption (Quantachrome Instruments, Autosorb AS-6B).

Electrochemical measurements: Electrochemical measurements were conducted by using two-electrode Swagelok-type cells with pure lithium foil as the counter and reference electrode at room temperature. The working electrode consisted of SnO_2 hollow nanostructures, carbon black (Super-P-Li), and polyvinylidene difluoride (PVDF) in a weight ratio of 7:2:1. The electrolyte used was 1.0 M $LiPF_6$ in a 50:50 (w/w) mixture of ethylene carbonate and diethyl carbonate. Cell assembly was carried out in an Ar-filled glovebox with concentrations of moisture and oxygen below 1.0 ppm. Galvanostatic charge–discharge tests were performed with a Neware battery tester at different current densities within a cutoff voltage window of 0.01–1.2 V. 1 C is equivalent to 782 mA g^{-1}, corresponding to 4.4 Li atoms per SnO_2 molecule.

Results and Discussion

The synthesis strategy for the formation of SnO_2 hollow nanostructures is illustrated in Scheme 1. In an acidic solution, the hydrolysis of Sn^{2+} is partially suppressed but can occur at a relatively high temperature to generate insoluble SnO_2 according to the following reaction [Eqs. (1) and (2)]:

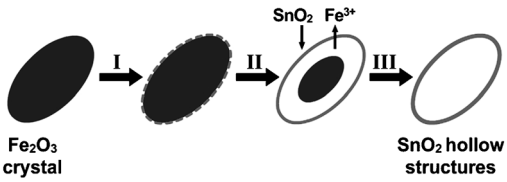

Scheme 1. Schematic illustration of the formation of SnO_2 hollow nanostructures: I) heterogeneous nucleation of SnO_2 grains around the scaffold of Fe_2O_3 crystals; II) continuous growth of SnO_2 shells and simultaneous dissolution of Fe_2O_3 cores by acidic etching; and III) formation of SnO_2 hollow structures after complete consumption of Fe_2O_3 crystals.

$$2Sn^{2+}_{(aq)} + 2H_2O + O_{2(g)} \rightarrow 2SnO_{2(s)} + 4H^{+}_{(aq)} \quad (1)$$

$$Fe_2O_3 + 6H^{+} \xrightarrow{\Delta} 2Fe^{3+} + 3H_2O \quad (2)$$

Because of mutual crystallographic compatibility, it is favorable for SnO_2 grains to heterogeneously nucleate around the scaffold of Fe_2O_3 crystals to decrease the system free energy and further evolve to a precipitation layer as a result of continuous crystal growth. Simultaneously, gradual disso-

lution of Fe_2O_3 templates also takes place due to thermally accelerated acidic etching in solution [Eq. (2)]. Although the rates of SnO_2 precipitation and Fe_2O_3 dissolution are comparable, SnO_2 hollow nanostructures with well-defined interiors and compact shells are eventually formed after complete consumption of Fe_2O_3 templates.

The crystallographic structure and phase purity of SnO_2 hollow nanostructures were determined by powder XRD, as shown in Figure 1. All the diffraction peaks can be perfectly

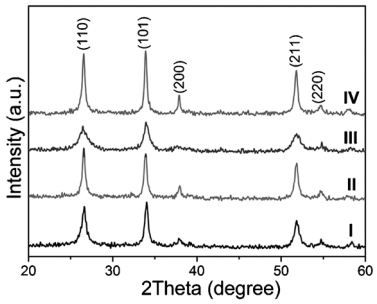

Figure 1. XRD patterns of SnO_2 hollow nanostructures with different shapes: I) nanococoons; II) nanoboxes; III) nanospheres; IV) nanorings.

assigned to tetragonal SnO_2 (JCPDS no. 41-1445) without noticeable signals from the impurities. The morphology and structure of the products were then examined by FESEM and TEM. As an example, Figure 2a–c shows the FESEM images of the product synthesized by templating against Fe_2O_3 nanospindles. A panoramic view reveals that this sample is entirely composed of high-quality nanococoons without impurity particles or aggregates. The nanococoons inherit well the uniform dimensions of Fe_2O_3 nanospindles with a size of around 300 nm. Their interior space can be examined directly from cracked nanococoons, as shown in Figure 2c. The hollow interior and geometrical structure of as-synthesized SnO_2 nanococoons are further elucidated by TEM, as displayed in Figure 2d–f. The SnO_2 nanococoons duplicate the spindle-like morphology of the Fe_2O_3 templates and the surface is relatively smooth without obvious defects. In agreement with the FESEM findings, a high uniformity of the nanococoons can be seen from the TEM images. Moreover, the inner cavities are clearly revealed by the sharp contrast between SnO_2 shells and hollow interiors. The wall of the nanococoons is as thin as about 10–15 nm, in favor of the precisely controlled precipitation of SnO_2 in an acidic solution. Selected-area electron diffraction (SAED) analysis indicates that the SnO_2 nanococoons are polycrystalline in nature (Figure 2g). The TEM images at higher magnifications depict the shell structure of the nanococoons (Figure 2h and i). Interestingly, it appears that there are some small pores with a size of several nanometers in the shell. The formation of such pores may be ascribed to the outward flow of Fe^{3+} ions upon the dissolution of Fe_2O_3 cores, which thus endows the nanococoons with highly permeable shells for efficient mass transport. The porous structure is further characterized by N_2 sorption measurement (see below).

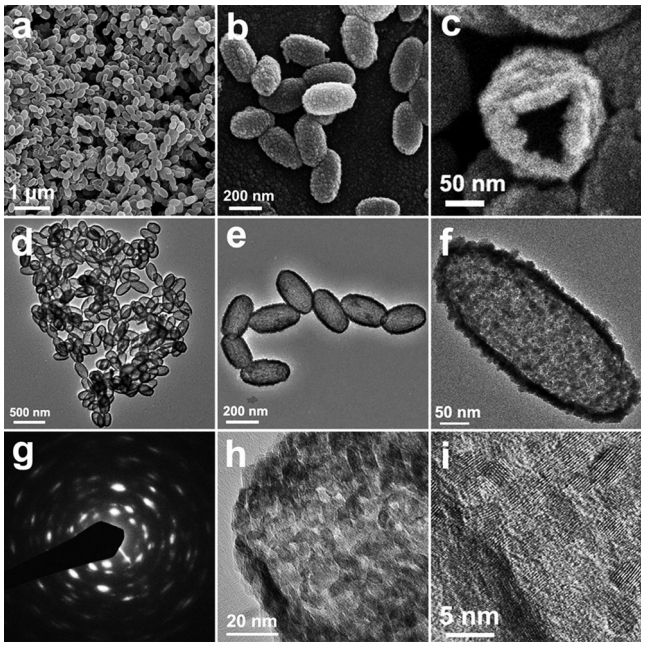

Figure 2. a) Overview FESEM image of SnO_2 nanococoons; b) several nanococoons with uniform dimensions; c) a cracked nanococoon showing the exposed interior; d) low-magnification TEM image of SnO_2 nanococoons; e) enlarged image of several nanococoons; f) a nanococoon with well-defined interior and compact thin shell; g) SAED pattern of SnO_2 nanococoons; h) the shell structure of the nanococoons; i) high-resolution TEM image of a nanococoon (scale bars: a) 1 μm; b) 200 nm; c) 50 nm; d) 500 nm; e) 200 nm; f) 50 nm; h) 20 nm; i) 5 nm).

To investigate the mechanism involved in the growth of SnO_2 nanococoons, the time course for the reaction was recorded by TEM, as shown in Figure 3. After reaction for 2 h, SnO_2 nanoparticles are formed on the surface of Fe_2O_3

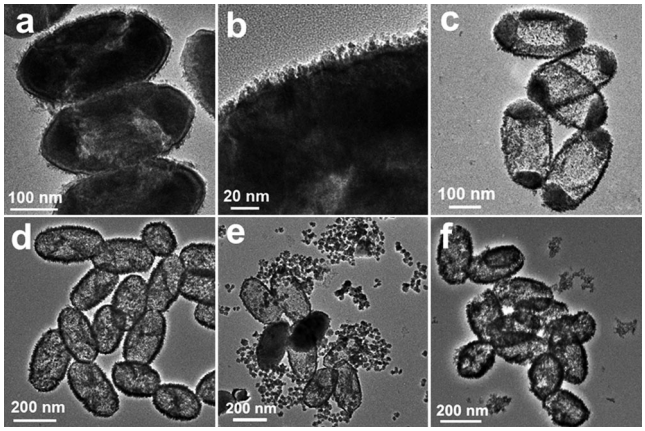

Figure 3. a–d) TEM images of SnO_2 nanococoons synthesized with different reaction durations of a, b) 2, c) 10, and d) 15 h. e, f) TEM images of the nanococoons obtained with 2 and 5 mL of hydrochloric acid added to the reaction system, respectively (scale bars: a) 100 nm; b) 20 nm; c) 100 nm; d) 200 nm; e) 200 nm; f) 200 nm).

nanospindles by heterogeneous nucleation (Figure 3a and b). Upon prolonging the reaction time to 5 h, continuous SnO_2 shells start to form around the scaffold of Fe_2O_3 nanospindles while the Fe_2O_3 cores are partially dissolved by acidic etching (Figure 3c). After reaction for 15 h, most of the Fe_2O_3 template is eliminated and SnO_2 nanococoons with completely hollow interiors are eventually obtained after 20 h. In this process, controlling the concentration of hydrochloric acid is crucial for the formation of SnO_2 hollow structures, because it kinetically controls the dissolution of Fe_2O_3 templates and the hydrolysis of Sn^{2+} ions. A lower concentration of hydrochloric acid, for example 0.25 M, leads to incomplete dissolution of Fe_2O_3 templates but much faster hydrolysis of Sn^{2+} ions. Large quantities of impurity particles are therefore formed as a result of homogeneous growth of SnO_2 nanocrystals in solution. In the presence of higher concentrations of hydrochloric acid, such as 0.60 M, only nanococoons with many defects are obtained due to insufficient deposition of SnO_2. When an excess amount (>0.70 M) of hydrochloric acid is introduced, little solid product can be obtained because of strong inhibition of hydrolysis of Sn^{2+} ions and complete dissolution of Fe_2O_3 templates. Apparently, the fine-tuned interplay between the hydrolysis of $SnCl_2$ and acidic etching of Fe_2O_3 templates is critical for the formation of SnO_2 hollow particles with perfect structures.

The physiochemical properties of hollow structures are not only highly dependent on the intrinsic crystalline texture and surface properties, but also greatly related to their morphological characteristics. The present approach provides the feasibility to rationally tailor the shape and size of SnO_2 hollow particles obtained by simply templating against pregrown Fe_2O_3 crystals with diverse shapes and sizes. For example, polycrystalline SnO_2 nanoboxes with smooth thin shells and uniform edge length of around 400 nm have been successfully synthesized with Fe_2O_3 nanocubes as shape-directing templates, as shown in Figure 4. Moreover, SnO_2 hollow nanorings and nanospheres could also be produced by templating against the respective Fe_2O_3 templates, although the shell quality is not as good as that of the structures obtained from spindle-like or cubic templates (Figure 5). We attribute this to the difficulty in kinetic control of the reactions over smaller templates with increased reactivity. In general, many metal salts with appropriate capability of hydrolysis can serve as potential precursors for the shell construction by the present strategy. A perhaps obvious appeal of our approach is that it can be readily extended to generate hollow nanostructures of other metal oxides, such as TiO_2, by simply replacing $SnCl_2$ with the desired shell precursors. Analogous to SnO_2 hollow structures, the obtained anatase TiO_2 nanococoons and nanoboxes (JCPDS no. 21-1272) also possess well-defined interiors and polycrystalline shells as a result of precisely controlled precipitation of TiO_2 on the entire surface of Fe_2O_3 crystals, as shown in Figure 6.

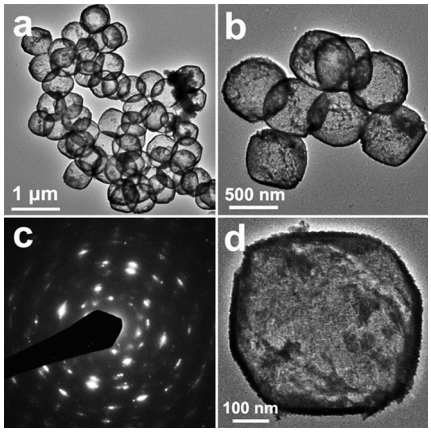

Figure 4. TEM images of SnO_2 nanoboxes: a) low-magnification image; b) several nanoboxes showing well-defined interiors; c) SAED pattern of SnO_2 nanoboxes; d) a nanobox with well-defined interior and compact thin shell (scale bars: a) 1 μm; b) 500 nm; d) 100 nm).

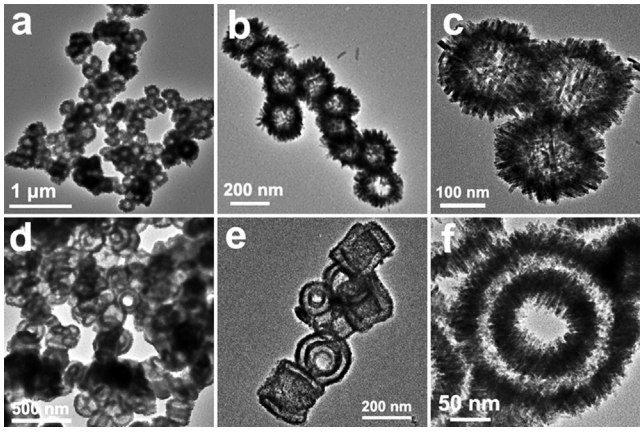

Figure 5. TEM images of a–c) SnO_2 hollow nanospheres and d–f) hollow nanorings (scale bars: a) 1 μm; b) 200 nm; c) 100 nm; d) 500 nm; e) 200 nm; f) 50 nm).

SnO_2 is a very appealing candidate as a substitute for the conventional graphite-based anode in LIBs because of its many attributes, including high theoretical capacity (782 mAh g^{-1}), nontoxicity, improved safety, and ready availability at low cost.[18,19,33] Generally, the electrochemical process of SnO_2 electrodes can be described by the following principal reactions [Eqs. (3) and (4)]:[18]

$$SnO_2 + 4Li^+ + 4e^- \rightarrow Sn + 2Li_2O \quad (3)$$

$$Sn + xLi^+ + xe^- \leftrightarrow Li_xSn\ (0 \le x \le 4.4) \quad (4)$$

The first reaction [Eq. (3)] is irreversible, and is the major cause of a large initial capacity loss during the first few charge–discharge cycles. The second alloying/dealloying process [Eq. (4)] is highly reversible but inherently causes huge and uneven volume variations within the electrode upon repeated lithium uptake/extraction. This results in electrode pulverization and electrical connectivity loss, which eventu-

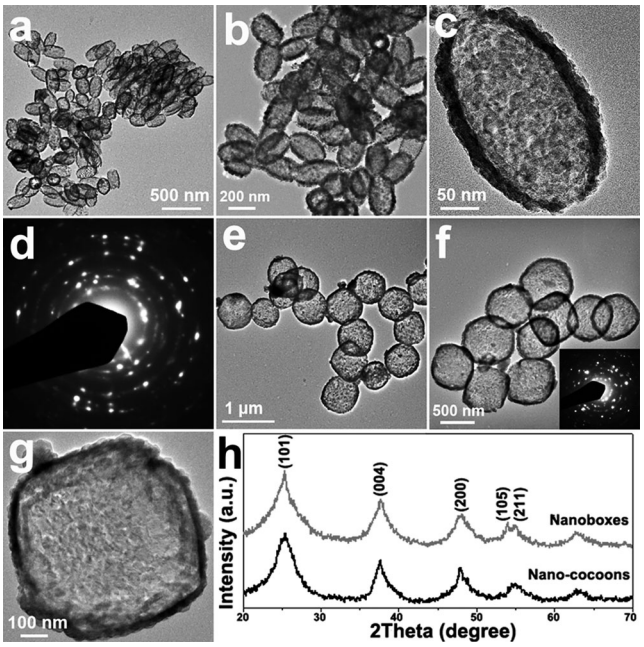

Figure 6. a–c) TEM images and d) SAED pattern of TiO_2 nanococoons; e–g) TEM images of TiO_2 nanoboxes; h) XRD profiles of the TiO_2 hollow structures (scale bars: a) 500 nm; b) 200 nm; c) 50 nm; e) 1 μm; f) 500 nm; g) 100 nm).

ally lead to poor cycling capability. One possible way to effectively mitigate this problem is to pass the SnO_2 materials from bulk to nanoscale hollow structures with enhanced kinetics and structural stability for lithium storage.[19,56,61] The as-synthesized SnO_2 hollow particles, including nanococoons, nanoboxes, hollow nanorings, and nanospheres, possess relatively large Brunauer–Emmett–Teller (BET) surface areas of 73, 82, 58, and 71 $m^2 g^{-1}$, respectively (Figure 7). The large surface area reasonably endows them with a higher capacity and favorable response to high-rate cycling relative to the bulk counterpart owing to a dramatic increment of reactive sites and interface between active materials and the electrolyte. From the isotherms, there exist porous structures in the shells as indicated by the hysteresis loops. The presence of permeable thin walls makes Li^+ ion diffusion much easier by shortening the diffusion length effectively to the grain size (typically a few nanometers). The interior space allows the volume variation upon lithium insertion/extraction to be better accommodated.

Motivated by the great promise of hollow structures in LIBs, we evaluated the electrochemical properties of the obtained SnO_2 hollow nanostructures. Figure 8a shows some representative discharge–charge voltage profiles of SnO_2 nanococoons at a 0.2 C rate within a cutoff voltage window of 0.01–1.2 V. The initial discharge and charge capacities are found to be 2020 and 640 mAh g^{-1}, respectively. The large capacity loss in the first cycle is mainly attributed to the initial irreversible formation of Li_2O [Eq. (3)], and other irreversible processes, such as trapping of some lithium in the lattice and inevitable formation of a solid electrolyte interface (SEI) layer, which are common for most anode materials.[17–20,32,48,51,57] Also, it is partly because the electrode is charged up to 1.2 V only in the present work. From the second cycle onwards, the nanostructures deliver capacities of over 760 mAh g^{-1} with stable capacity retention of about 91% for over 50 cycles (Figure 8b). This value is much higher than the theoretical capacity of graphite (372 mAh g^{-1}). For commercial SnO_2 nanoparticles, the capacity decays rapidly to less than 300 mAh g^{-1} within only 20 cycles, also shown in Figure 8b. In addition to the cycling stability, high-rate capability is also generally considered important, especially for high-power LIBs. Benefiting from the unique hollow structures, SnO_2 nanococoons exhibit improved cycling response to the gradually increasing current rates, although SnO_2 is known to suffer from sluggish kinetics. Even cycled at higher rates of 0.5–1 C, comparable capacities of 450–620 mAh g^{-1} can still be delivered, as shown in Figure 8c. After fast cycling at 1 C, a stable capacity of around 750 mAh g^{-1} can still be restored when the current density is reduced back to 0.2 C. To demonstrate the general advantages of SnO_2 hollow nanostructures for lithium storage, the cycling performance of the other three types of SnO_2 hollow particles were also investigated under the same conditions (Figure 8d). For SnO_2 nanoboxes,

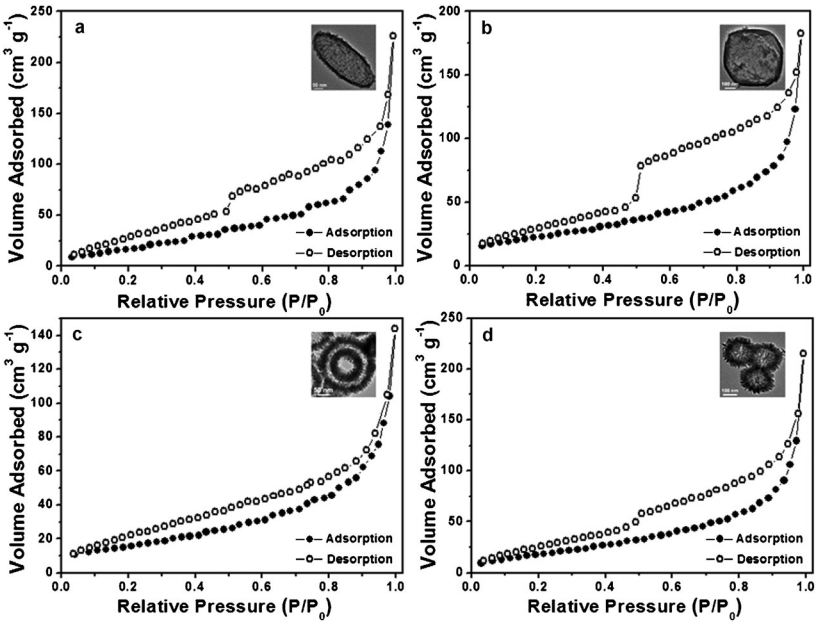

Figure 7. N_2 adsorption/desorption isotherms of SnO_2 hollow nanostructures with various shapes.

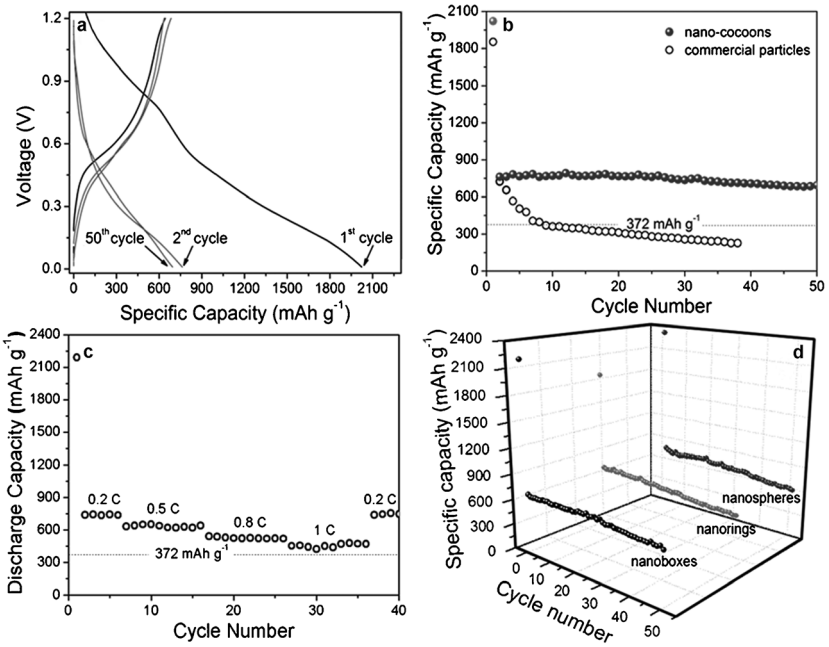

Figure 8. a) Discharge–charge voltage profiles of SnO_2 nanococoons at 0.2 C; b) cycling performance of SnO_2 nanococoons and commercial SnO_2 particles at 0.2 C; c) rate capability of SnO_2 nanococoons at various current rates; d) cycling ability of SnO_2 nanoboxes, hollow nanorings, and nanospheres at 0.2 C. For all tests, the cutoff voltage window is 0.01–1.2 V.

hollow nanorings, and nanospheres, high capacities of 671, 611, and 593 mAh g^{-1} can be retained after 50 cycles, and all of them exhibit stable capacity retention of over 80% after the second cycle despite the different shapes. The performance of all of them is superior to that of bulk solid particles. It appears that the formation of hollow nanostructures is beneficial to the improved lithium storage capability of SnO_2 materials due to the substantial advantages of the large electrode/electrolyte interface, shortened charge/Li^+ diffusion length, and enhanced structural stability. In this sense, the design and construction of hollow nanostructures can arguably provide an effective route towards high-performance SnO_2-based anodes for next-generation LIBs.

Conclusion

The strategy demonstrated in this work provides a facile and general route for one-step preparation of metal oxide hollow nanostructures by templating against shape-controlled α-Fe_2O_3 crystals under hydrothermal conditions. The strategy allows the morphology and composition of the resultant hollow particles to be rationally tailored. As a demonstration, uniform SnO_2 and TiO_2 hollow structures with designed shapes, such as nanococoons, nanoboxes, hollow nanorings, and nanospheres, have been successfully prepared. The interplay of acidic etching of Fe_2O_3 templates and precisely controlled hydrolysis of precursor (e.g., $SnCl_2$ and TiF_4) is important for the formation of these high-quality hollow structures. When evaluated as anode materials for LIBs, the SnO_2 hollow nanostructures exhibit stable capacities of 600–700 mAh g^{-1} over 50 cycles at a 0.2 C rate and good rate capability at 0.5–1 C due to greatly enhanced structural stability and kinetics for lithium storage. Consistent with many previous reports, the findings reported herein might suggest the promising use of hollow structures in high-performance LIBs. Besides LIBs, these SnO_2 and TiO_2 hollow structures are likely to find applications in solar cells, sensors, and catalysis.

Acknowledgements

The authors are grateful to the National Research Foundation (Singapore) for financial support through the Clean Energy Research Programme (CERP; NRF2009EWTCERP001-036).

[1] X. W. Lou, L. A. Archer, Z. C. Yang, *Adv. Mater.* **2008**, *20*, 3987.
[2] M. R. Langille, M. L. Personick, J. Zhang, C. A. Mirkin, *J. Am. Chem. Soc.* **2011**, *133*, 10414.
[3] J. Lee, J. C. Park, H. Song, *Adv. Mater.* **2008**, *20*, 1523.
[4] Y. F. Zhu, J. L. Shi, W. H. Shen, X. P. Dong, J. W. Feng, M. L. Ruan, Y. S. Li, *Angew. Chem.* **2005**, *117*, 5213; *Angew. Chem. Int. Ed.* **2005**, *44*, 5083.
[5] S. E. Skrabalak, J. Y. Chen, Y. G. Sun, X. M. Lu, L. Au, C. M. Cobley, Y. N. Xia, *Acc. Chem. Res.* **2008**, *41*, 1587.
[6] Y. G. Sun, B. Wiley, Z. Y. Li, Y. N. Xia, *J. Am. Chem. Soc.* **2004**, *126*, 9399.
[7] M. L. Pang, J. Y. Hu, H. C. Zeng, *J. Am. Chem. Soc.* **2010**, *132*, 10771.
[8] A. M. Cao, J. S. Hu, H. P. Liang, L. J. Wan, *Angew. Chem.* **2005**, *117*, 4465; *Angew. Chem. Int. Ed.* **2005**, *44*, 4391.
[9] Z. Y. Zhong, Y. D. Yin, B. Gates, Y. N. Xia, *Adv. Mater.* **2000**, *12*, 206.
[10] S. W. Kim, M. Kim, W. Y. Lee, T. Hyeon, *J. Am. Chem. Soc.* **2002**, *124*, 7642.
[11] F. Caruso, R. A. Caruso, H. Mohwald, *Science* **1998**, *282*, 1111.
[12] M. Yang, J. Ma, C. Zhang, Z. Yang, Y. Lu, *Angew. Chem.* **2005**, *117*, 6885; *Angew. Chem. Int. Ed.* **2005**, *44*, 6727.
[13] C. I. Zoldesi, A. Imhof, *Adv. Mater.* **2005**, *17*, 924.
[14] Q. Peng, Y. J. Dong, Y. D. Li, *Angew. Chem.* **2003**, *115*, 3135; *Angew. Chem. Int. Ed.* **2003**, *42*, 3027.
[15] N. A. Dhas, K. S. Suslick, *J. Am. Chem. Soc.* **2005**, *127*, 2368.
[16] Z. Y. Wang, D. Y. Luan, C. M. Li, F. B. Su, S. Madhavi, F. Y. C. Boey, X. W. Lou, *J. Am. Chem. Soc.* **2010**, *132*, 16271.
[17] S. J. Ding, J. S. Chen, G. G. Qi, X. N. Duan, Z. Y. Wang, E. P. Giannelis, L. A. Archer, X. W. Lou, *J. Am. Chem. Soc.* **2011**, *133*, 21.
[18] X. W. Lou, C. M. Li, L. A. Archer, *Adv. Mater.* **2009**, *21*, 2536.
[19] X. W. Lou, Y. Wang, C. Yuan, J. Y. Lee, L. A. Archer, *Adv. Mater.* **2006**, *18*, 2325.
[20] Z. Y. Wang, D. Y. Luan, F. Y. C. Boey, X. W. Lou, *J. Am. Chem. Soc.* **2011**, *133*, 4738.
[21] M. Chen, L. Wu, S. Zhou, B. You, *Adv. Mater.* **2006**, *18*, 801.

[22] Z. Yang, Z. Niu, Y. Lu, Z. Hu, C. C. Han, *Angew. Chem.* **2003**, *115*, 1987; *Angew. Chem. Int. Ed.* **2003**, *42*, 1943.
[23] X. W. Lou, C. L. Yuan, L. A. Archer, *Adv. Mater.* **2007**, *19*, 3328.
[24] Y. G. Sun, B. T. Mayers, Y. N. Xia, *Nano Lett.* **2002**, *2*, 481.
[25] Y. M. Sui, W. Y. Fu, Y. Zeng, H. B. Yang, Y. Y. Zhang, H. Chen, Y. X. Li, M. H. Li, G. T. Zou, *Angew. Chem.* **2010**, *122*, 4378; *Angew. Chem. Int. Ed.* **2010**, *49*, 4282.
[26] C. H. Kuo, M. H. Huang, *J. Am. Chem. Soc.* **2008**, *130*, 12815.
[27] K. An, S. G. Kwon, M. Park, H. Bin Na, S. I. Baik, J. H. Yu, D. Kim, J. S. Son, Y. W. Kim, I. C. Song, W. K. Moon, H. M. Park, T. Hyeon, *Nano Lett.* **2008**, *8*, 4252.
[28] H. L. Cao, X. F. Qian, C. Wang, X. D. Ma, J. Yin, Z. K. Zhu, *J. Am. Chem. Soc.* **2005**, *127*, 16024.
[29] S. H. Jiao, L. F. Xu, K. Jiang, D. S. Xu, *Adv. Mater.* **2006**, *18*, 1174.
[30] X. G. Han, M. S. Jin, S. F. Xie, Q. Kuang, Z. Y. Jiang, Y. Q. Jiang, Z. X. Xie, L. S. Zheng, *Angew. Chem.* **2009**, *121*, 9344; *Angew. Chem. Int. Ed.* **2009**, *48*, 9180.
[31] E. R. Leite, I. T. Weber, E. Longo, J. A. Varela, *Adv. Mater.* **2000**, *12*, 965.
[32] Y. Wang, H. C. Zeng, J. Y. Lee, *Adv. Mater.* **2006**, *18*, 645.
[33] C. Wang, Y. Zhou, M. Y. Ge, X. B. Xu, Z. L. Zhang, J. Z. Jiang, *J. Am. Chem. Soc.* **2010**, *132*, 46.
[34] M. Law, H. Kind, B. Messer, F. Kim, P. D. Yang, *Angew. Chem.* **2002**, *114*, 2511; *Angew. Chem. Int. Ed.* **2002**, *41*, 2405.
[35] J. Z. Wang, N. Du, H. Zhang, J. X. Yu, D. R. Yang, *J. Phys. Chem. C* **2011**, *115*, 11302.
[36] J. J. Zhu, Z. H. Lu, S. T. Aruna, D. Aurbach, A. Gedanken, *Chem. Mater.* **2000**, *12*, 2557.
[37] Y. K. Liu, C. L. Zheng, W. Z. Wang, C. R. Yin, G. H. Wang, *Adv. Mater.* **2001**, *13*, 1883.
[38] Y. L. Wang, X. C. Jiang, Y. N. Xia, *J. Am. Chem. Soc.* **2003**, *125*, 16176.
[39] D. F. Zhang, L. D. Sun, J. L. Yin, C. H. Yan, *Adv. Mater.* **2003**, *15*, 1022.
[40] B. Cheng, J. M. Russell, W. S. Shi, L. Zhang, E. T. Samulski, *J. Am. Chem. Soc.* **2004**, *126*, 5972.
[41] Y. Liu, H. Dong, M. L. Liu, *Adv. Mater.* **2004**, *16*, 353.
[42] L. Vayssieres, M. Graetzel, *Angew. Chem.* **2004**, *116*, 3752; *Angew. Chem. Int. Ed.* **2004**, *43*, 3666.
[43] H. G. Yang, H. C. Zeng, *Angew. Chem.* **2004**, *116*, 6056; *Angew. Chem. Int. Ed.* **2004**, *43*, 5930.
[44] S. J. Han, B. C. Jang, T. Kim, S. M. Oh, T. Hyeon, *Adv. Funct. Mater.* **2005**, *15*, 1845.
[45] D. F. Zhang, L. D. Sun, C. J. Jia, Z. G. Yan, L. P. You, C. H. Yan, *J. Am. Chem. Soc.* **2005**, *127*, 13492.
[46] J. H. He, T. H. Wu, C. L. Hsin, K. M. Li, L. J. Chen, Y. L. Chueh, L. J. Chou, Z. L. Wang, *Small* **2006**, *2*, 116.
[47] M. S. Park, G. X. Wang, Y. M. Kang, D. Wexler, S. X. Dou, H. K. Liu, *Angew. Chem.* **2007**, *119*, 764; *Angew. Chem. Int. Ed.* **2007**, *46*, 750.
[48] Z. H. Wen, Q. Wang, Q. Zhang, J. H. Li, *Adv. Funct. Mater.* **2007**, *17*, 2772.
[49] Y. Yu, C. H. Chen, Y. Shi, *Adv. Mater.* **2007**, *19*, 993.
[50] R. Demir-Cakan, Y. S. Hu, M. Antonietti, J. Maier, M. M. Titirici, *Chem. Mater.* **2008**, *20*, 1227.
[51] X. W. Lou, D. Deng, J. Y. Lee, L. A. Archer, *Chem. Mater.* **2008**, *20*, 6562.
[52] M. S. Park, Y. M. Kang, G. X. Wang, S. X. Dou, H. K. Liu, *Adv. Funct. Mater.* **2008**, *18*, 455.
[53] D. Deng, M. G. Kim, J. Y. Lee, J. Cho, *Energy Environ. Sci.* **2009**, *2*, 818.
[54] J. F. Qian, P. Liu, Y. Xiao, Y. Jiang, Y. L. Cao, X. P. Ai, H. X. Yang, *Adv. Mater.* **2009**, *21*, 3663.
[55] H. X. Zhang, C. Feng, Y. C. Zhai, K. L. Jiang, Q. Q. Li, S. S. Fan, *Adv. Mater.* **2009**, *21*, 2299.
[56] J. F. Ye, H. J. Zhang, R. Yang, X. G. Li, L. M. Qi, *Small* **2010**, *6*, 296.
[57] S. J. Ding, J. S. Chen, D. Y. Luan, F. Y. C. Boey, S. Madhavi, X. W. Lou, *Chem. Commun.* **2011**, *47*, 7155.
[58] M. Ozaki, S. Kratohvil, E. Matijevic, *J. Colloid Interface Sci.* **1984**, *102*, 146.
[59] J. S. Chen, T. Zhu, C. M. Li, X. W. Lou, *Angew. Chem.* **2011**, *123*, 676; *Angew. Chem. Int. Ed.* **2011**, *50*, 650.
[60] C. J. Jia, L. D. Sun, F. Luo, X. D. Han, L. J. Heyderman, Z. G. Yan, C. H. Yan, K. Zheng, Z. Zhang, M. Takano, N. Hayashi, M. Eltschka, M. Klaui, U. Rudiger, T. Kasama, L. Cervera-Gontard, R. E. Dunin-Borkowski, G. Tzvetkov, J. Raabe, *J. Am. Chem. Soc.* **2008**, *130*, 16968.
[61] K. T. Lee, Y. S. Jung, S. M. Oh, *J. Am. Chem. Soc.* **2003**, *125*, 5652.

Received: December 7, 2011
Revised: February 17, 2012
Published online: April 26, 2012

